



Title	Photocatalytic hydrogen generation with simultaneous organic degradation by a visible light-driven CdS/ZnS film catalyst
Author(s)	Wang, X; Li, XY
Citation	Materials Science and Engineering B: Solid-State Materials for Advanced Technology, 2014, v. 181 n. 1, p. 86-92
Issued Date	2014
URL	http://hdl.handle.net/10722/202679
Rights	NOTICE: this is the author's version of a work that was accepted for publication in Materials Science and Engineering B: Solid-State Materials for Advanced Technology. Changes resulting from the publishing process, such as peer review, editing, corrections, structural formatting, and other quality control mechanisms may not be reflected in this document. Changes may have been made to this work since it was submitted for publication. A definitive version was subsequently published in Materials Science and Engineering B: Solid-State Materials for Advanced Technology, 2014, v. 181 n. 1, p. 86-92. DOI: 10.1016/j.mseb.2013.11.015

Re-submitted to: Materials Science and Engineering B (MSB-D-13-00826)

Date: October 18, 2013

Photocatalytic hydrogen generation with simultaneous organic degradation by a visible light-driven CdS/ZnS film catalyst

Xi Wang^{1,2} and Xiao-yan Li^{2*}

¹ School of Chemistry and Environment, South China Normal University, Guangzhou, Guangdong, China

² Environmental Engineering Research Centre, Department of Civil Engineering, The University of Hong Kong, Pokfulam Road, Hong Kong

(*Corresponding author: phone: 852 2859-2659; fax: 852 2859-5337; e-mail: xlia@hkucc.hku.hk)

Abstract

1
2 A layered CdS/ZnS catalyst film was synthesized on glass using the stepped chemical bath
3 deposition method. The film catalyst was shown as visible light-driven photocatalyst
4 capable of producing H₂ under visible light. The ZnS outer layer helped suppress the
5 recombination of photo-generated electron-hole pairs on the CdS base layer, leading to
6 faster H₂ generation. The use of the ZnS layer also greatly improved the stability of the
7 catalyst film and prevented the leaching of Cd²⁺ from the CdS layer. Deposition of Ru on
8 the catalyst film further increased its photoreactivity for H₂ production. The photocatalyst
9 was effective in H₂ production together with the degradation of model organic substances,
10 such as formic acid, methanol, and ethanol. The greatest H₂ production rates were achieved

11 using the CdS/ZnS/Ru film in the formic acid solution at $123 \mu\text{mol}/\text{m}^2\text{-h}$ under visible light
12 and $135 \text{ mmol}/\text{m}^2\text{-h}$ under the simulated solar light. The corresponding theoretical reduction
13 rates of chemical oxygen demand (COD) were 1.9 and $2.1 \text{ g}/\text{m}^2\text{-h}$, respectively. As the
14 multilayer CdS/ZnS/Ru film catalyst can be easily separated from water, it has a great
15 potential for simultaneous photocatalytic hydrogen generation and organic wastewater
16 treatment using solar energy.

17

18 **Keywords:** CdS-ZnS, hydrogen generation, organic degradation, photolysis, photocatalyst
19 film, solar energy.

20

21 **1. Introduction**

22 Hydrogen is one of the most promising forms of clean and renewable energy.
23 Photocatalytic hydrogen generation from water is an attractive and environmentally friendly
24 method to harvest solar energy [1, 2]. However, while visible light ($\lambda > 420 \text{ nm}$) covers a large
25 portion of the solar spectrum, most photocatalysts, such as TiO_2 , function only under
26 energy-intensive ultraviolet (UV) irradiation. Efforts have been made in recent years to
27 develop photocatalysts, such as metal oxides (e.g. ZnO) and metal sulfides (e.g. CdS), that
28 respond to both UV and visible lights for water photolysis [3]. However, most photocatalysts
29 are still hampered by typical problems such as the recombination of photo-generated
30 electron-hole pairs [4] and low stability of the catalysts due to photo-corrosion [5-7].

31 In addition to hydrogen evolution (H^+ reduction), photocatalytic reactions in water
32 possess a strong oxidation power that may be utilized for pollutant degradation [8, 9].
33 During the photocatalytic process under solar light, pollutants such as sulfide and organic
34 matters [3, 10], including alcohols [11-15] and organic acids [6, 15, 16], can function as
35 electron donors for hydrogen evolution, while the pollutants are degraded. In such a

36 photocatalytic application, the purposes of both hydrogen generation and wastewater
37 treatment using solar energy can be achieved [6, 9].

38 Most visible light-driven photocatalysts are produced and applied in a powder form.
39 However, for potential application in wastewater treatment, an easy separation of the
40 photocatalysts from the treated effluent is required. Hence, there are efforts made to
41 immobilize photocatalysts in solid carriers to eliminate the need for separation in the
42 treatment process [17-20]. However, few studies have been conducted on the use of
43 film-type catalysts for photocatalytic hydrogen production together with organic pollutant
44 degradation [21-23]. In our previous study, composite CdS/ZnS nanoparticles were
45 synthesized as a visible light-driven photocatalyst for H₂ production [24]. The present work
46 aims to develop a multilayer film-type CdS/ZnS catalyst that can achieve both photocatalytic
47 H₂ production and organic degradation under the simulated solar light or visible light.

48

49 **2. Materials and Methods**

50 *2.1 Preparation of the CdS/ZnS thin film catalysts*

51 Microscopic glass slides were used as the base material for the deposition of the
52 CdS/ZnS catalyst films. The catalyst was deposited on both sides of a slide with a
53 dimension of $2.5 \times 5.5 \text{ cm}^2$. The glass slides were cleaned thoroughly with detergent,
54 degreased with ethanol in an ultrasonic cleaner, and then etched in 4% HNO₃ solution. The
55 chemical bath deposition (CBD) process was used to deposit the catalyst material on the
56 glass surface. The CdS coating solution was prepared using an aqueous solution of 0.005 M
57 Cd(NO₃)₂ in a 0.005 M NH₄NO₃ buffer mixed with 0.06 M thiourea (SC(NH₂)₂). The pH of
58 the coating solution was adjusted to 8.5-9.5 using 25% NH₄OH. During the deposition
59 process, the glass slides were immersed in the coating solution in a beaker, which was then
60 placed in a water bath heated to 50 °C. The CBD process lasted for 30 min to allow CdS

61 deposition. The CdS film on the glass was then annealed at 450 °C for 1 h in a furnace (LHT
62 02/16 LBR, Nabertherm) supplied with pure nitrogen.

63 The outer ZnS layer was coated following the same CBD procedures. The ZnS coating
64 solution was prepared in an aqueous solution of 0.04 M Zn(NO₃)₂ with was chelated with
65 0.04×²/₃ tri-sodium citrate (Na₃C₆H₅O₇) mixed with 0.06 M thiourea, and the solution pH
66 was adjusted to 10 [25]. The glass slides with the CdS film were immersed in the solution
67 for ZnS deposition in a water bath at 50 °C for different CBD periods (1, 2, and 3 h).
68 Accordingly, the catalyst films were denoted as CdS/ZnS-1h, CdS/ZnS-2h, and CdS/ZnS-3h
69 for the different ZnS coating periods. The glass slides coated with the catalyst film were
70 then annealed at 450 °C for 1 h. The amount of CdS/ZnS coated on the slide surface was
71 calculated by the weight increase after the catalyst coating.

72 Ruthenium (Ru) was deposited on the surface of the catalyst film by *in-situ*
73 photodeposition in a 10% (vol) acetic acid (CH₃COOH) solution of RuCl₃ (Aldrich). The
74 photodeposition was conducted by illuminating ($\lambda > 420$ nm, 300 W Xe lamp) the CdS/ZnS
75 film for 20 min in 150 mL of the coating solution with a Ru concentration of 53.5 mg/L. For
76 CdS/ZnS-2h, the catalyst layer on the slide weighed about 800 mg. According to the
77 concentration measurement, nearly all Ru³⁺ in the solution (8.025 mg) deposited on the
78 slide after the photodeposition. Thus, the resulting Ru deposition density was approximately
79 1.0 wt% (i.e. ~8 mg vs. ~800 mg) of the catalyst coating layer of CdS/ZnS-2h. The catalyst
80 film with Ru deposition was denoted as CdS/ZnS/Ru.

81

82 2.2 Characterization of the film photocatalysts

83 The amount (mass) of the film catalyst that was coated on a glass slide was determined
84 from the weight increase after each step of the chemical deposition. The crystalline phase
85 and structural features of the catalysts were analyzed using an X-ray diffraction (XRD)

86 system (D8 Advance, Burker AXS) with Cu K α irradiation from 10-90 degrees. The diffuse
87 reflection spectrum (DRS) of the catalyst film was obtained using a UV-vis
88 spectrophotometer (Lambda 25, Perkin Elmer) that was converted from the reflection
89 function to the absorbance function following the Kubelka-Munk method [26]. The
90 morphology of the thin catalyst film was examined under a scanning electron microscope
91 (SEM, Hitachi S-4800 FEG), and the thickness of the catalyst film on the glass surface was
92 measured using an atomic force microscope (AFM, BioMAT™ Workstation).

93

94 *2.3 Photocatalytic H₂ production with different model organic pollutants under* 95 *visible light*

96 The photocatalytic hydrogen production experiments were conducted in a cylindrical
97 photo cell made of optical glass. A 300 W Xe lamp setup (PLS-SXE Xe light source,
98 Trustech) was used as the light source with a cutoff filter ($\lambda < 420$ nm) installed to provide
99 visible light (denoted by Vis, light intensity ~ 70 mW/cm²) and without a cutoff filter to
100 simulate the solar light (denoted by Solar, light intensity ~ 86 mW/cm²). Two pieces of the
101 glass slides with the catalyst film were placed next to each other in the photo cell filled with
102 150 mL of water or an organic solution. The light was applied from the top of the photo cell
103 on a total catalyst film area of 27.5 cm². Different model organic pollutants (formic acid,
104 methanol, and ethanol) were tested for the photocatalytic H₂ production and organic
105 degradation experiments. The solution had an organic content of 10% by volume and was
106 kept at pH \sim 7. The gas produced during the photo-tests was collected, and its hydrogen and
107 carbon dioxide contents were determined using a gas chromatograph (HP5890 Series II,
108 Hewlett Packard). Each run of the photo-test lasted approximately 4 h. The reactivity of the
109 photocatalyst in different solutions was evaluated in terms of the specific hydrogen

110 production rate (R) and energy conversion efficiency (η), as determined by the following
111 equations:

$$112 \quad R_A = \frac{m_{H_2}}{A t}, \text{ or} \quad (1)$$

$$113 \quad R_w = \frac{m_{H_2}}{W t}, \text{ and} \quad (2)$$

$$114 \quad \eta = \frac{R \Delta H_c}{I}, \quad (3)$$

115 where R_A and R_w are the area-based and weight-based specific H_2 production rates,
116 respectively, m_{H_2} is the moles of the H_2 produced, t is the duration of the photoreaction, A is
117 the irradiation area (27.5 cm^2), W is the amount (weight) of the catalyst in the photocell for
118 H_2 generation, ΔH_c is the combustion value of H_2 (286 kJ/mol), and I is the light density. The
119 photocatalytic H_2 generation test was repeated 10 times for each catalyst film under an
120 experimental condition to evaluate the reproducibility of the experiment and the stability of
121 the film catalyst. In addition, the amount of Cd^{2+} leaching into the water during the
122 photocatalytic experiments was measured using an atomic absorption spectrometer (AAAnalyst
123 300, Perkin Elmer).

124

125 **3 Results and Discussion**

126 *3.1 Synthesis and optimization of the double-layer film catalysts*

127 The coating solution's pH was found to control the rate of CdS deposition and the
128 quality of the coating layer on glass (Fig. 1). The rate of CdS deposition generally increased
129 as pH increased. As shown by the SEM images, the deposition was slow at pH 8.5 and the
130 surface coating was not completed in 30 min. At pH 9.0, the CdS deposition film was not
131 uniformly distributed on the glass and the coating quality was unsatisfactory. At pH 9.5, the

132 coating quality greatly improved and a smooth and uniform deposition layer was obtained
133 with a thickness of approximately 150 nm, according to the AFM measurement.

134 During the coating process, the precursor reaction on the substrate surface leads to
135 heterogeneous precipitation and the resulting film formation on the base substrate. The
136 precipitation of CdS on the glass surface, or $Cd^{2+} + S^{2-} \rightleftharpoons CdS(s)$, was controlled by the
137 concentrations of free Cd^{2+} and S^{2-} in the coating solution. In this study, NH_3 was chosen as
138 the complexing agent for Cd^{2+} , which released a small amount of Cd^{2+} according to the
139 complexion dissociation, i.e. $[Cd(NH_3)_n]^{2+} \rightleftharpoons Cd^{2+} + nNH_3$. The NH_3 concentration was
140 related to pH and its equilibrium constant ($K_{NH_3, H_2O} = 1.79 \times 10^{-5}$). Meanwhile, the free S^{2-}
141 released from hydrolysis of thiourea was also controlled by the solution pH, according to
142 $SC(NH_2)_2 + OH^- \rightleftharpoons SH^- + CN_2H_2 + H_2O$ and $SH^- + OH^- \rightleftharpoons S^{2-} + H_2O$. At pH 8.5, the
143 hydrolysis of thiourea was slow, which hindered the deposition of CdS on the glass [27].
144 When the pH was increased to 9.0, the hydrolysis of thiourea became faster. However, due
145 to the low NH_3 level (0.0027 M based on its equilibrium constant), a high concentration of
146 free Cd^{2+} resulted in a rapid CdS precipitation on the glass surface and in the bulk solution.
147 This facilitated a cluster-by-cluster deposition to form a thick and non-uniform coating layer
148 on the glass surface. The coating layer was loose and could easily peel from the surface. At
149 pH 9.5, a smooth and uniform CdS film was formed on the glass with adequate NH_3
150 (0.0088 M) chelating Cd^{2+} and sufficient hydrolysis of thiourea. The film growth rate and
151 thickness were moderate, for which the heterogeneous 'ion by ion' deposition was expected
152 at the surface with a low potential of film cracking [28]. Thus, pH 9.5 was chosen for the
153 deposition of the inner CdS layer.

154 The ZnS layer was deposited by the similar chelating system at pH 10 to form a
155 condensed film [25]. The ZnS growth rate was controlled by the deposition temperature.
156 The morphology of ZnS and CdS layers and their interface was examined by SEM (Fig. S3,

157 Supporting Material). At a low temperature of 40 °C, the ZnS deposited on the CdS surface
158 was thin, uneven and loose, which could easily fall off from the surface. At a high
159 temperature of 60 °C, the ZnS film was thick and the interface was loose. At 50 °C, the best
160 film deposition quality could be achieved with a compact ZnS layer and its firm adhesion to
161 the inner CdS layer.

162 The outer ZnS layer was found to affect the photo-reactivity of the CdS/ZnS film
163 catalyst. For photocatalytic H₂ production with formic acid as the model organic, hydrogen
164 was produced by the single layer CdS film, and no hydrogen was produced by the single
165 ZnS layer under the visible light and simulated solar light (Fig. 2). Deposition of ZnS on the
166 CdS layer did not reduce its H₂ production activity. On the contrary, the ZnS outer layer
167 significantly increased the H₂ production rate of the photocatalyst film. With the ZnS
168 coating for 2 h, the double-layer film catalyst CdS/ZnS-2h achieved the highest H₂
169 production rate of 31.2 μmol/h under visible light and 45.9 μmol/h under the solar light,
170 which is three times of that obtained with the single-layer CdS film. However, further
171 increasing the ZnS coating period to 3 h resulted in no additional increase of the H₂
172 production rate.

173

174 3.2 Characterization of the double-layer CdS/ZnS thin film photocatalyst

175 The inner CdS and outer ZnS layers can be well identified on the glass slides (Fig. 3).
176 The base CdS formed a dense layer on the glass with an average thickness of about 150 nm
177 as measured by the AFM. The outer layer of CdS/ZnS-2h had an average thickness of 125
178 nm consisting of fine ZnS particles. The XRD analysis indicated different crystal phases of
179 the CdS/ZnS film catalyst (Fig. 4). For instance, three XRD peaks at scattering angles (2θ)
180 of 26.5°, 43.8°, and 52.0° could be indexed to the diffractions of the cubic CdS crystal
181 lattice (JCPDS Card No. 75-1546), of which the peaks at 26.5° and 52.0° are associated

182 with only the cubic phase. The XRD peak at 36.5° is associated with only the hexagonal
183 CdS phase. ZnS crystalline phase appears at $2\theta = 28.7^\circ, 48.4^\circ,$ and 56.4° , which are close to
184 the values reported for cubic ZnS (JCPDS card No. 5-0566).

185 The diffuse reflection spectra of the single-layer CdS and ZnS films and the
186 double-layer CdS/ZnS film displayed the photo-sensitivity of the catalyst films (Fig. 5). As
187 expected, single-layer ZnS did not responded to visible light. CdS responded well to visible
188 light with a narrow band-gap of 2.23 eV determined from the absorbance edge in Fig. 5. For
189 the double-layer CdS/ZnS film, its absorbance increased greatly in the low wavelength range
190 of visible light in comparison to the single ZnS layer. The ZnS coating on the CdS film also
191 resulted in a slight blue shift of the absorbance edge compared to the single-layer CdS film.
192 The double-layer CdS/ZnS film had a band-gap of 2.45 eV, suggesting a similar response as
193 the CdS film to visible light.

194 While CdS responses to visible light, ZnS adsorbs only UV irradiation. However, when
195 ZnS was deposited on CdS to form a composite CdS/ZnS thin film, the reactivity of the
196 photocatalyst increased clearly as suggested by the photo-test results. There is an apparent
197 synergistic effect between the two catalyst materials for the photocatalytic process. The use
198 of the more photoreactive CdS layer ensured the reactivity and efficiency of the catalyst film
199 under visible light [24]. Moreover, the sensitive CdS would function as a photo-sensitizer to
200 induce the excitation of ZnS that was in direct contact with CdS. The higher conduction band
201 and lower valence band of ZnS demonstrate the heterojunction of ZnS/CdS. In this case, this
202 heterojunction can establish fast transport channels along with efficient eh separation and
203 effectively suppress the electron loss at the CdS surface. As shown in Fig. S1
204 (Supplementary Material), the electron flow through the heterojunction between CdS and
205 ZnS is important to the effective electron-hole separation. Similar photoelectrical
206 mechanisms have been identified for quantum-dot sensitized solar cells [29, 30]. Under solar

207 light, the excited electron of ZnS outer layer injected in to the CB of CdS increased the
208 electron flow to the surface and helped suppress the recombination of electron-hole pairs
209 formed in the CdS inner layer, making the electrons more available for H₂ evolution as
210 show in Fig. S1 [14, 15].

211 The use of the outer ZnS layer also improved the stability of the CdS-based
212 photocatalyst under either the visible light or simulated solar light. After 10 runs of the
213 photo-H₂ tests, the composite double-layer catalyst retained 90% of its H₂-producing
214 capability under visible light, while the single-layer CdS film retained only 52% of its
215 reactivity for H₂ production (Fig. 6A). A similar comparison of the test results was also
216 observed under the solar light between the photocatalyst films with and without the ZnS
217 layer (Fig. 6B).

218 The ZnS outer layer also prevented the leaching of Cd²⁺ from the catalyst film during
219 the photocatalytic process. Between test runs 2 and 5, the CdS/ZnS-2h catalyst had an
220 average Cd²⁺ leaching rate of 24.7 μg/h under visible light, while the single-layer CdS film
221 had a Cd²⁺ leaching rate of 73.7 μg/h (Fig. 6A). Between runs 6 and 10, the leaching of
222 Cd²⁺ from CdS/ZnS-2h diminished to a rate of 1.2 μg/h compared to the CdS film with a
223 Cd²⁺ leaching rate of 24.3 μg/h. The similar results were obtained with the same catalyst
224 films under solar light (Fig. 6B). Use of the outer ZnS layer physically separated CdS from
225 the reaction medium to protect the more reactive CdS layer against photo-corrosion.

226 The adhesion and stability of the coating films are of extremely importance to the
227 performance of the film catalyst. The quality of the catalyst films was regularly assessed by
228 manual examination and visual and SEM observations during the synthesis process and the
229 photocatalytic hydrogen production tests. After a number of test runs, the aqueous solution
230 remained clean and clear, and the SEM images also showed the compact morphology of the
231 films (Fig. S2, Supporting Material). There was no sign of the films peeling off from the slide

232 surface. The thickness and roughness of the films before and after the hydrogen production
233 tests were also detected by the AFM, and the results presented in [Table S1](#) (Supporting
234 Material) show little changes of the photocatalyst films (the thickness remained at ~150 nm
235 with a roughness of ~13 nm). As reported in Fig. 6, after 10 runs of the photo-H₂ tests, the
236 composite catalyst film retained 90% of its H₂-producing capability under visible light. All of
237 these indicate the good quality and stability of the catalyst films deposited on the glass slides.

238

239 *3.3 Hydrogen production with simultaneous organic degradation*

240 The CdS/ZnS film catalyst was capable of both photocatalytic H₂ production and
241 organic degradation under visible light and solar light ([Fig. 7A](#)). The H₂ production rate
242 increased for the model organic pollutants in an order of ethanol, methanol, and formic acid.
243 For the photocatalyst films in pure water, no hydrogen was produced in the absence of the
244 model organics even under the solar light. The photocatalyst was apparently unable to split
245 water to produce hydrogen under visible light or solar light. However, the presence of
246 organic matters enabled the photocatalyst to produce hydrogen from water. The model
247 organic pollutants function as electron donors for the reduction of H⁺ ions, giving rise to H₂
248 evolution.

249 Moreover, the Ru deposition on the catalyst surface resulted in a 10-fold increase in H₂
250 production rate. As Ru possesses a lower Fermi energy level than CdS/ZnS [31], it would
251 function as an electron collector at the surface of the CdS/ZnS film for the electrochemical
252 process. The photo-excited electrons could readily transfer from the photocatalyst to the Ru
253 sites on the catalyst surface. Such an electron collection would facilitate the electron transfer
254 from CdS/ZnS to H⁺ ions in the aqueous solution for H₂ evolution. In other words, Ru
255 deposition on the CdS/ZnS surface helps the charge separation on the catalyst, resulting in
256 improved H₂ generation [32].

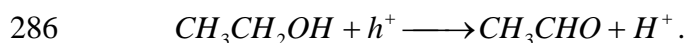
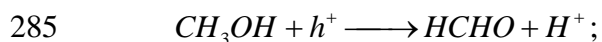
257 The highest H₂ production rate under visible light was achieved at 123 mmol/m²-h
258 with the CdS/ZnS/Ru film in formic acid, with an energy conversion efficiency of 1.41%.
259 The highest H₂ production rate under the simulated solar light was 135 mmol/m²-h in
260 formic acid, with an energy conversion efficiency of 1.26%. In relation to H⁺ reduction for
261 H₂ production, the corresponding organic degradation in terms of the chemical oxygen
262 demand (COD) removal may be estimated using the following formula:

$$263 \quad COD \text{ removal} = \frac{m_{H_2} M_{O_2}}{2} \quad (4)$$

264 where M_{O₂} is the molar mass of O₂ (32 g/mol). The theoretical photocatalytic COD reduction
265 rates for formic acid by the CdS/ZnS/Ru film were 5.4 mg/h in visible light and 6.0 mg/h in
266 solar light (Fig. 7B), corresponding to area-based-specific rates of 1.9 and 2.1 g COD/m²-h,
267 respectively. Degradation of formic acid resulted in CO₂ production. During the
268 photocatalytic test, CO₂ was generated at a rate of 73 mmol/m²-h in the gaseous phase, which
269 agrees well with the theoretical COD reduction rate of formic acid. The molar ratio of H₂ to
270 CO₂ produced was approximately 1:1, suggesting a complete decomposition of formic acid. It
271 is believed that formic acid (E⁰_{CO₂/HCOOH} = -0.126 V) functioned as an electron donor to trap
272 photo-generated holes on the valence band of CdS/ZnS [33], resulting in the organic
273 decomposition and CO₂ production.

274 The hydrogen production rates in the methanol and ethanol solutions under visible light
275 were 104 and 92 mmol/m²-h, respectively, which are higher than that reported by Daskalaki
276 et al. [34] for the Pt/CdS/TiO₂ film catalyst. Hydrogen production from 10% ethanol
277 achieved an energy conversion efficiency of 1.04% in visible light, which is also higher
278 than the efficiency reported by [35] for the Pt/TiO₂ film catalyst in 80% ethanol under UV
279 irradiation. Nonetheless, CO₂ production was not detected during the photocatalytic H₂
280 generation in both methanol and ethanol solutions. It is apparent that the photocatalytic
281 reactions resulted in organic destruction and intermediate formation other than complete

282 organic mineralization [14, 36]. When the CdS/ZnS film catalyst was excited in visible light,
283 the photo-generated holes would attack methanol and ethanol to produce methanal and
284 ethanal, respectively, according to the following reactions [14, 37]:



287 The composite CdS/ZnS double-layer film structure exhibited a synergetic function of
288 the catalyst materials for photocatalytic H₂ generation and organic degradation. Moreover,
289 as described previously, film-type photocatalysts can be easily separated from water or
290 solutions for repeated use. This property is particularly important in wastewater treatment
291 applications. The catalyst film also allows better light penetration compared with the
292 suspension of catalyst powders [38]. The CdS/ZnS/Ru film catalyst had a
293 weight-based-specific H₂ production rate of up to 8.5 mmol/g-h for visible light irradiation,
294 which was higher than that of the CdS/ZnS/Ru catalyst powders. This implies that the
295 photocatalyst film is as good as catalyst powders in utilizing visible light or solar light for
296 H₂ production. Together with its immobilized feature, the multilayer CdS/ZnS/Ru film
297 catalyst demonstrates a great more potential for simultaneous photocatalytic H₂ production
298 and wastewater organic degradation.

299

300 **4 Conclusions**

- 301 • The double-layer CdS/ZnS film catalyst was synthesized by chemical bath deposition
302 for photocatalytic H₂ production under visible light. The ZnS outer layer helps suppress
303 the recombination of photo-generated electron-hole pairs on the more photosensitive
304 CdS base layer, leading to a faster H₂ production rate. Moreover, compared with the
305 single-layer CdS film, the use of ZnS in the double-layer CdS/ZnS film greatly

306 improved the stability of the catalyst and prevented the leaching of Cd^{2+} from the
307 catalyst film.

- 308 • The visible light-driven photocatalyst was capable of both producing hydrogen and
309 degrading model organic pollutants (formic acid, methanol, and ethanol). The
310 CdS/ZnS/Ru film had an H_2 production rate of $123 \text{ mmol/m}^2\text{-h}$ in the formic acid
311 solution with an energy conversion efficiency of 1.41%. In relation to H_2 production, the
312 theoretical COD reduction rate for formic acid was $1.9 \text{ g COD/m}^2\text{-h}$ by the catalyst film
313 under visible light.
- 314 • As the multilayer CdS/ZnS/Ru catalyst film is well immobilized and can be easily
315 separated from water, it presents a great potential in both photocatalytic H_2 generation
316 and organic wastewater treatment using solar energy.

317

318 **Acknowledgments**

319 This research was supported by grants HKU714112E from the Research Grants Council
320 (RGC) and SEG_HKU10 from the University Grants Committee (UGC) of the Government
321 of Hong Kong SAR, and #51308230 from the National Natural Science Foundation of
322 China (NSFC). The technical assistance of Mr. Keith C.H. Wong is highly appreciated.

323

324 **References:**

- 325 [1] K. Maeda, K. Teramura, D.L. Lu, T. Takata, N. Saito, Y. Inoue, K. Domen, Photocatalyst
326 releasing hydrogen from water - enhancing catalytic performance holds promise for
327 hydrogen production by water splitting in sunlight., *Nature* 440 (2006) 295.
- 328 [2] C. Grimes, O.K. Varghese, S. Ranjan, *Light, water, hydrogen: the solar generation of*
329 *hydrogen by water photoelectrolysis*, Springer, New York, USA, 2008.

- 330 [3] P. Lianos, Production of electricity and hydrogen by photocatalytic degradation of
331 organic wastes in a photoelectrochemical cell: The concept of the Photofuelcell: A
332 review of a re-emerging research field, *J. Hazard. Mater.* 185 (2011) 575-590.
- 333 [4] M.T. Lee, M. Werhahn, D.J. Hwang, N. Hotz, R. Greif, D. Poulikakos, C.P.
334 Grigoropoulos, Hydrogen production with a solar steam-methanol reformer and colloid
335 nanocatalyst, *Int. J. Hydrogen Energy* 35 (2010) 118-126.
- 336 [5] M. Law, L.E. Greene, A. Radenovic, T. Kuykendall, J. Liphardt, P.D. Yang, ZnO-Al₂O₃
337 and ZnO-TiO₂ core-shell nanowire dye-sensitized solar cells, *J. Phys. Chem. B* 110
338 (2006) 22652-22663.
- 339 [6] X. Zong, H.J. Yan, G.P. Wu, G.J. Ma, F.Y. Wen, L. Wang, C. Li, Enhancement of
340 photocatalytic H₂ evolution on CdS by loading MoS₂ as cocatalyst under visible light
341 irradiation, *J. Am. Chem. Soc.* 130 (2008) 7176-7177.
- 342 [7] H. Yan, J. Yang, G. Ma, G. Wu, X. Zong, Z. Lei, J. Shi, C. Li, Visible-light-driven
343 hydrogen production with extremely high quantum efficiency on Pt-PdS/CdS
344 photocatalyst, *J. Catal.* 266 (2009) 165-168.
- 345 [8] A. Patsoura, D.I. Kondarides, X.E. Verykios, Photocatalytic degradation of organic
346 pollutants with simultaneous production of hydrogen, *Catal. Today* 124 (2007) 94-102.
- 347 [9] Y.J. Zhang, L. Zhang, Preparation of Ru-loaded CdS/Al-HMS nanocomposites and
348 production of hydrogen by photocatalytic degradation of formic acid, *Appl. Surf. Sci.*
349 255 (2009) 4863-4866.

- 350 [10] H. Park, A. Bak, Y.Y. Ahn, J. Choi, M.R. Hoffmann, Photoelectrochemical
351 performance of multi-layered BiO_x-TiO₂/Ti electrodes for degradation of phenol and
352 production of molecular hydrogen in water, *J. Hazard. Mater.* 211 (2012) 47-54.
- 353 [11] N.L. Wu, M.S. Lee, Z.J. Pon, J.Z. Hsu, Effect of calcination atmosphere on TiO₂
354 photocatalysis in hydrogen production from methanol/water solution, *J. Photochem.*
355 *Photobiol. B: Chem.* 163 (2004) 277-280.
- 356 [12] M. Zalas, M. Laniecki, Photocatalytic hydrogen generation over lanthanides-doped
357 titania, *Sol. Energy Mater. Sol. Cells* 89 (2005) 287-296.
- 358 [13] S.M. Ji, P.H. Borse, H.G. Kim, D.W. Hwang, J.S. Jang, S.W. Bae, J.S. Lee,
359 Photocatalytic hydrogen production from water-methanol mixtures using N-doped
360 Sr₂Nb₂O₇ under visible light irradiation: effects of catalyst structure, *Phys. Chem.*
361 *Chem. Phys.* 7 (2005) 1315-1321.
- 362 [14] J.P. Best, D.E. Dunstan, Nanotechnology for photolytic hydrogen production: colloidal
363 anodic oxidation, *Int. J. Hydrogen Energy* 34 (2009) 7562-7578.
- 364 [15] Y.W. Cao, U. Banin, Growth and properties of semiconductor core/shell nanocrystals
365 with InAs cores, *J. Am. Chem. Soc.* 122 (2000) 9692-9702.
- 366 [16] X.J. Zheng, L.F. Wei, Z.H. Zhang, Q.J. Jiang, Y.J. Wei, B. Xie, M.B. Wei, Research on
367 photocatalytic H₂ production from acetic acid solution by Pt/TiO₂ nanoparticles under
368 UV irradiation, *Int. J. Hydrogen Energy* 34 (2009) 9033-9041.

- 369 [17] C. Guillard, B. Beaugiraud, C. Dutriez, J.M. Herrmann, H. Jaffrezic, N.
370 Jaffrezic-Renault, M. Lacroix, Physicochemical properties and photocatalytic activities
371 of TiO₂ films prepared by sol-gel methods, *Appl. Catal. B: Env.* 39 (2002) 331-342.
- 372 [18] S. Zhou, A.K. Ray, Kinetic studies for photocatalytic degradation of eosin B on a thin
373 film of titanium dioxide, *Ind. Eng. Chem. Res.* 42 (2003) 6020-6033.
- 374 [19] G. Balasubramanian, D.D. Dionysiou, M.T. Suidan, I. Baudin, J.M. Laîné, Evaluating
375 the activities of immobilized TiO₂ powder films for the photocatalytic degradation of
376 organic contaminants in water, *Appl. Catal. B: Env.* 47 (2004) 73-84.
- 377 [20] K.L. Rosas-Barrera, J.A. Pedraza-Avella, B.P. Ballén-Gaitán, J. Cortés-Peña, J.E.
378 Pedraza-Rosas, D.A. Laverde-Cataño, Photoelectrolytic hydrogen production using
379 Bi₂MNbO₇ (M=Al, Ga) semiconductor film electrodes prepared by dip-coating, *Mater.*
380 *Sci. Eng. B* 176 (2011) 1359-1363.
- 381 [21] D.G. Diso, G.E.A. Muftah, V. Patel, I.M. Dharmadasa, Growth of CdS layers to develop
382 all-electrodeposited CdS/CdTe thin-film solar cells, *J. Electrochem. Soc.* 157 (2010)
383 H647-H651.
- 384 [22] N. Strataki, P. Lianos, Optimization of parameters for hydrogen production by
385 photocatalytic alcohol reforming in the presence of Pt/TiO₂ nanocrystalline thin films,
386 *J. Adv. Oxid. Technol.* 11 (2008) 111-115.
- 387 [23] S. Chun, K.S. Han, J.S. Lee, H.J. Lim, H. Lee, D. Kim, Fabrication CdS thin film and
388 nanostructure grown on transparent ITO electrode for solar cells, *Curr. Appl. Phys.* 10
389 (2010) S196-S200.

- 390 [24] X. Wang, K. Shih, X.Y. Li, Photocatalytic hydrogen generation from water under visible
391 light using core/shell nano-catalysts, *Water Sci. Technol.* 61 (2010) 2303-2308.
- 392 [25] A. Cheng, D.B. Fan, H. Wang, B.W. Liu, Y.C. Zhang, H. Yan, Chemical bath deposition
393 of crystalline ZnS thin films, *Semicond. Sci. Technol.* 18 (2003) 676-679.
- 394 [26] P. Kubelka, F. Munk, Ein Beitrag zur Optik der Far- banstriche, *Zeitschrift Technische*
395 *Physik* 12 (1931) 593-601.
- 396 [27] Q. Liu, G.B. Mao, Comparison of CdS and ZnS thin films prepared by chemical bath
397 deposition, *Surf. Rev. Lett.* 16 (2009) 469-474.
- 398 [28] T. Ye, Z. Suo, A.G. Evans, Thin-Film Cracking and the Roles of Substrate and Interface,
399 *International Journal of Solids and Structures* 29 (1992) 2639-2648.
- 400 [29] G. Hodes, Comparison of Dye- and Semiconductor-Sensitized Porous Nanocrystalline
401 Liquid Junction Solar Cells, *The Journal of Physical Chemistry C* 112 (2008)
402 17778-17787.
- 403 [30] S.W. Jung, J.-H. Kim, H. Kim, C.-J. Choi, K.-S. Ahn, ZnS overlayer on in situ chemical
404 bath deposited CdS quantum dot-assembled TiO₂ films for quantum dot-sensitized
405 solar cells, *Curr. Appl. Phys.* 12 (2012) 1459-1464.
- 406 [31] A. Kudo, M. Sekizawa, Photocatalytic H₂ evolution under visible light irradiation on
407 Ni-doped ZnS photocatalyst, *Chem. Commun.* (2000) 1371-1372.
- 408 [32] R. Dholam, N. Patel, A. Miotello, Efficient H₂ production by water-splitting using
409 indium-tin-oxide/V-doped TiO₂ multilayer thin film photocatalyst, *Int. J. Hydrogen*
410 *Energy* 36 (2011) 6519-6528.

- 411 [33] T. Chen, G. Wu, Z. Feng, G. Hu, W. Su, P. Ying, C. Li, In situ FT-IR study of
412 photocatalytic decomposition of formic acid to hydrogen on Pt/TiO₂ catalyst, Chinese J.
413 Catal. 29 (2008) 105-107.
- 414 [34] V.M. Daskalaki, M. Antoniadou, G.L. Puma, D.I. Kondarides, P. Lianos, Solar
415 light-responsive Pt/CdS/TiO₂ photocatalysts for hydrogen production and simultaneous
416 degradation of inorganic or organic sacrificial agents in wastewater, Environ. Sci.
417 Technol. 44 (2010) 7200-7205.
- 418 [35] N. Strataki, V. Bekiari, D.I. Kondarides, P. Lianos, Hydrogen production by
419 photocatalytic alcohol reforming employing highly efficient nanocrystalline titania
420 films, Appl. Catal. B: Env. 77 (2007) 184-189.
- 421 [36] Y. Lin, R.F. Lin, F. Yin, X.R. Xiao, M. Wu, W.Z. Gu, W.Z. Li, Photoelectrochemical
422 studies of H₂ evolution in aqueous methanol solution photocatalysed by Q-ZnS
423 particles, J. Photochem. Photobiol. B: Chem. 125 (1999) 135-138.
- 424 [37] G.L. Chiarello, L. Forni, E. Selli, Photocatalytic hydrogen production by liquid- and
425 gas-phase reforming of CH₃OH over flame-made TiO₂ and Au/TiO₂, Catal. Today 144
426 (2009) 69-74.
- 427 [38] M. Fathinia, A.R. Khataee, M. Zarei, S. Aber, Comparative photocatalytic degradation
428 of two dyes on immobilized TiO₂ nanoparticles: Effect of dye molecular structure and
429 response surface approach, J. Mol. Catal. A: Chem. 333 (2010) 73-84.
430
431

432 **Figure captions:**

433 **Fig. 1.** SEM micrographs of the CdS catalyst film deposited at (A) pH = 8.5, (B) pH = 9.0,
434 and (C) pH = 9.5 (left: cross-section; right: surface).

435 **Fig. 2.** Photocatalytic H₂ production under visible light or simulated solar light by the
436 catalyst films with different amounts of ZnS deposition. (ZnS-1h, ZnS-2h, and
437 ZnS-3h specify the duration (1, 2, and 3 h) of ZnS deposition on the catalyst films)

438 **Fig. 3.** SEM images of the double-layer CdS/ZnS thin film on glass (top: cross-section;
439 bottom, surface).

440 **Fig. 4.** XRD patterns of the CdS and the CdS/ZnS catalyst films (CdS-black square,
441 ZnS-open square).

442 **Fig. 5.** Diffuse reflection spectra of the double-layer CdS/ZnS film and the single-layer CdS
443 and ZnS films.

444 **Fig. 6.** Comparisons between the double-layer CdS/ZnS catalyst film and the single-layer
445 CdS film in terms of H₂ production, the stability of the photocatalytic reactivity, and
446 the rate of Cd²⁺ release under (A) visible light and (B) simulated solar light (each
447 test lasted 4 h).

448 **Fig. 7.** (A) Photocatalytic H₂ production and (B) the corresponding COD removal rate by
449 the CdS/ZnS and CdS/ZnS/Ru catalyst films in different organic solutions.

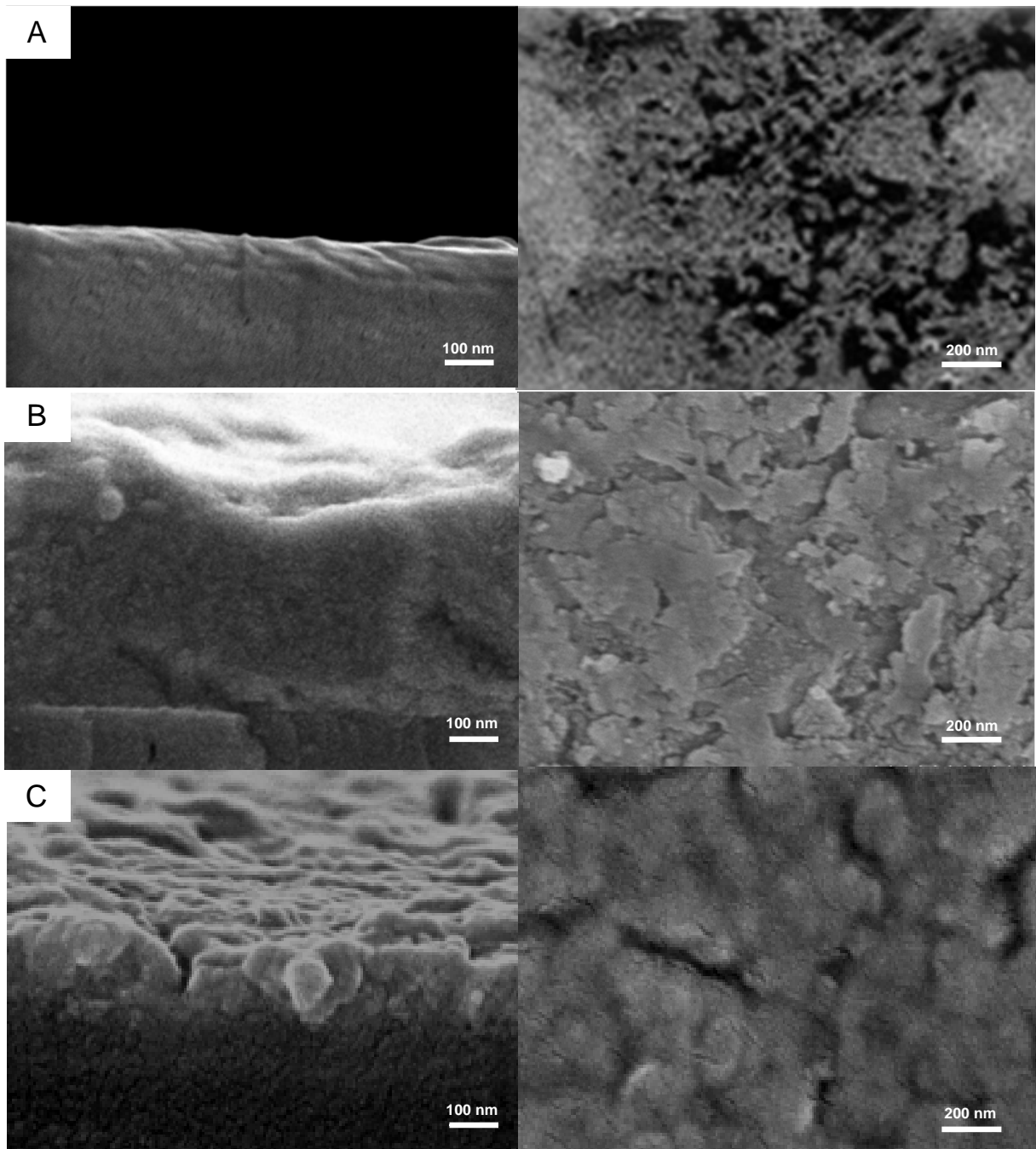


Fig. 1. SEM micrographs of the CdS catalyst film deposited at (A) pH = 8.5, (B) pH = 9.0, and (C) pH = 9.5 (left: cross-section; right: surface).

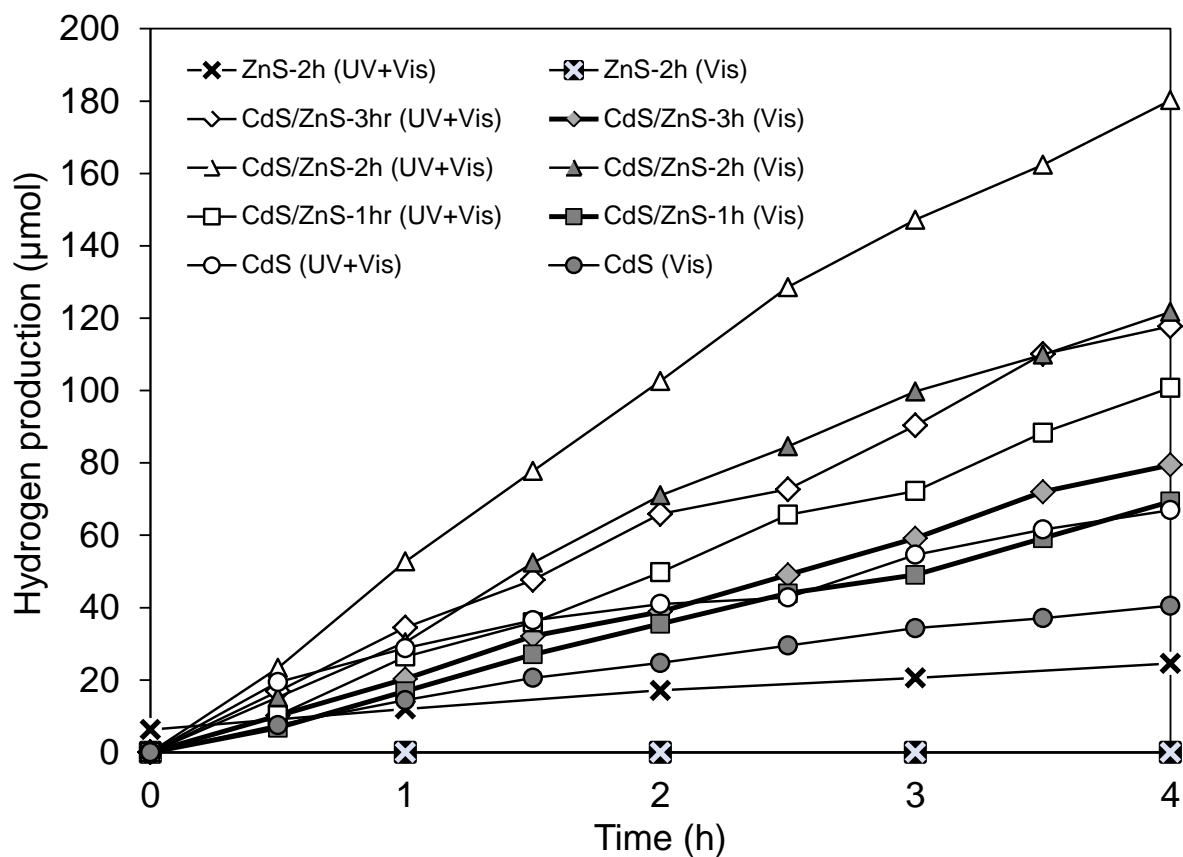


Fig. 2. Photocatalytic H₂ production under visible light or simulated solar light by the catalyst films with different amounts of ZnS deposition. (ZnS-1h, ZnS-2h, and ZnS-3h specify the duration (1, 2, and 3 h) of ZnS deposition on the catalyst films)

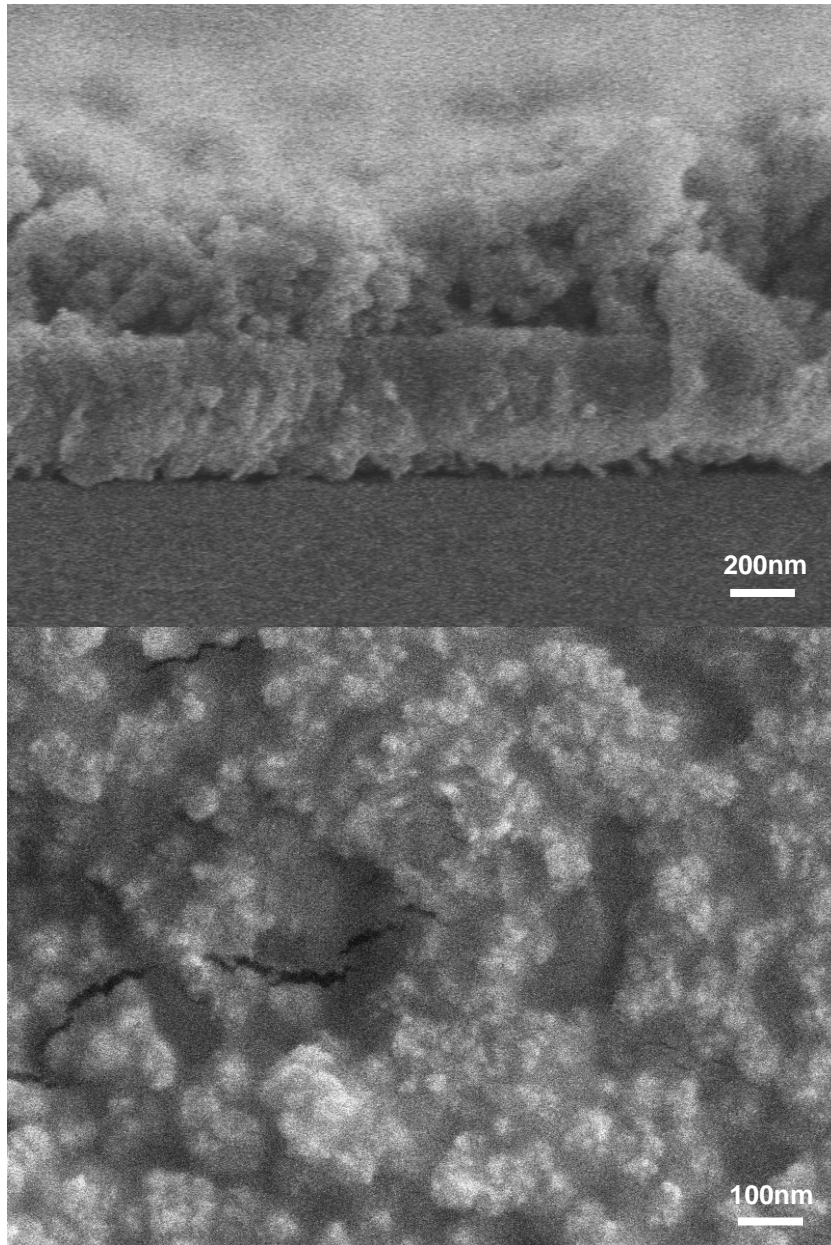


Fig. 3. SEM images of the double-layer CdS/ZnS thin film on glass (top: cross-section; bottom, surface).

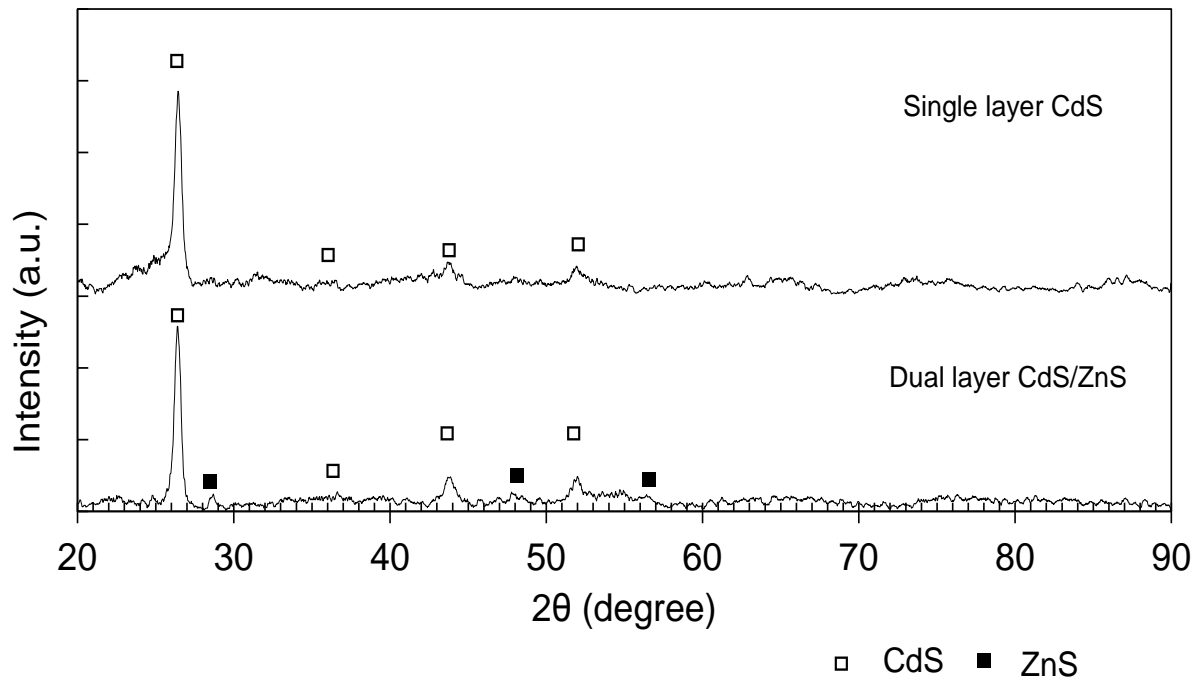


Fig. 4. XRD patterns of the CdS and the CdS/ZnS catalyst films (CdS-black square, ZnS-open square).

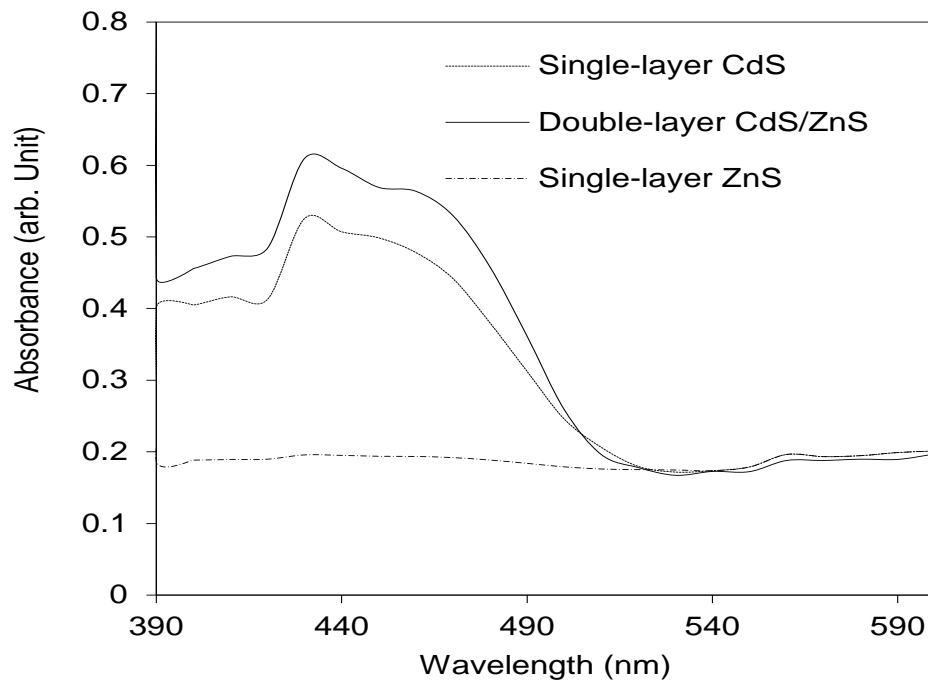


Fig. 5. Diffuse reflection spectra of the double-layer CdS/ZnS film and the single-layer CdS and ZnS films.

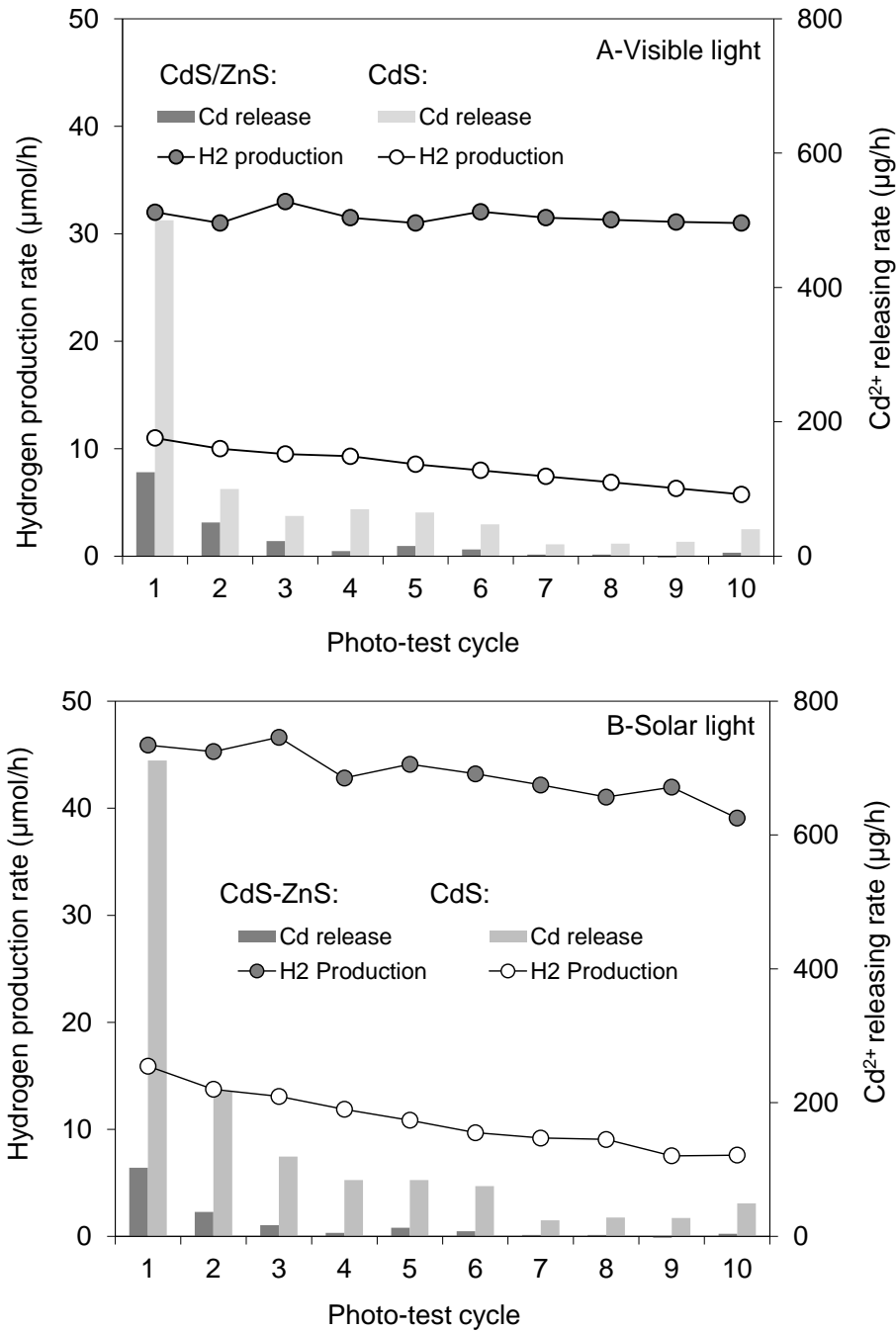


Fig. 6. Comparisons between the double-layer CdS/ZnS catalyst film and the single-layer CdS film in terms of H₂ production, the stability of the photocatalytic reactivity, and the rate of Cd²⁺ release under (A) visible light and (B) simulated solar light (each test lasted 4 h).

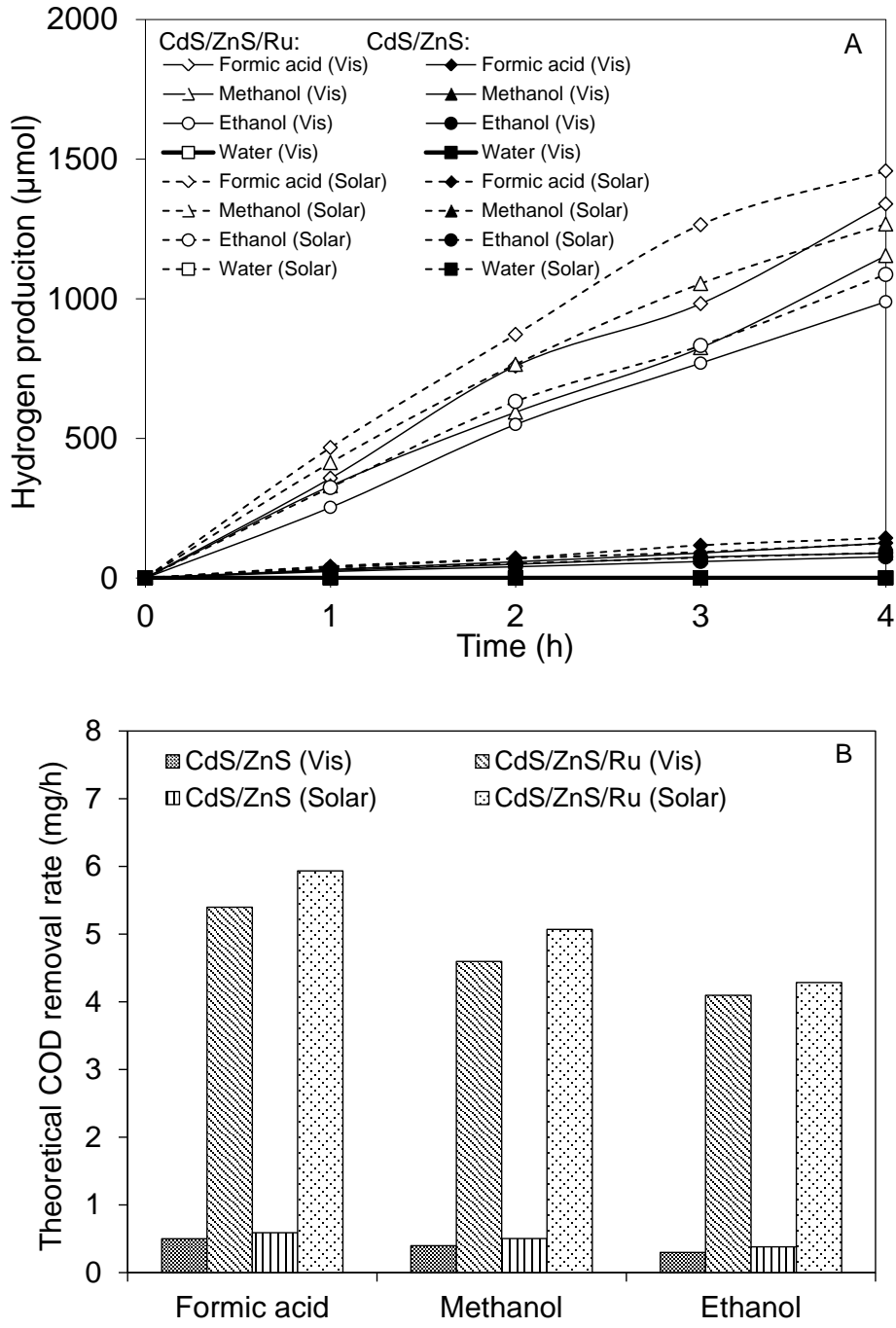


Fig. 7. (A) Photocatalytic H₂ production and (B) the corresponding COD removal rate by the CdS/ZnS and CdS/ZnS/Ru catalyst films in different organic solutions.

Supporting Material

Photocatalytic hydrogen generation with simultaneous organic degradation by a visible light-driven CdS/ZnS film catalyst

Xi Wang^{1,2} and Xiao-yan Li^{2*}

1 School of Chemistry and Environment, South China Normal University, Guangzhou, Guangdong, China

2 Environmental Engineering Research Centre, Department of Civil Engineering, The University of Hong Kong, Pokfulam Road, Hong Kong

(*Corresponding author: phone: 852 2859-2659; fax: 852 2859-5337; e-mail: xlia@hkucc.hku.hk)

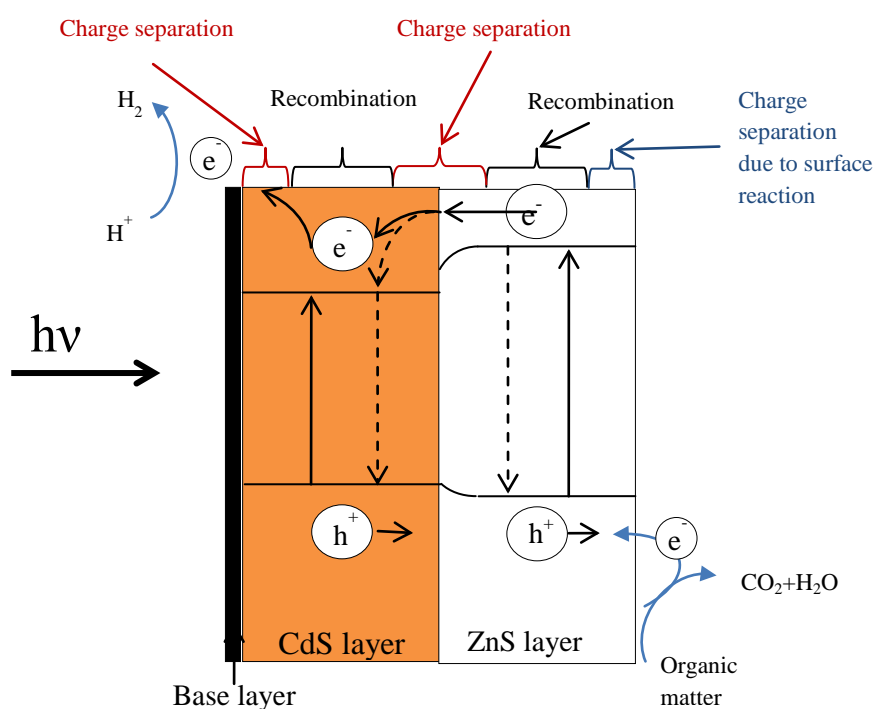


Fig. S1. Illustration of the synergistic effect of two-layer CdS/ZnS on photo-induced electron transfer and the resulting hydrogen evolution and organic degradation. (e^- and h^+ signify photo-induced electron and hole, respectively)

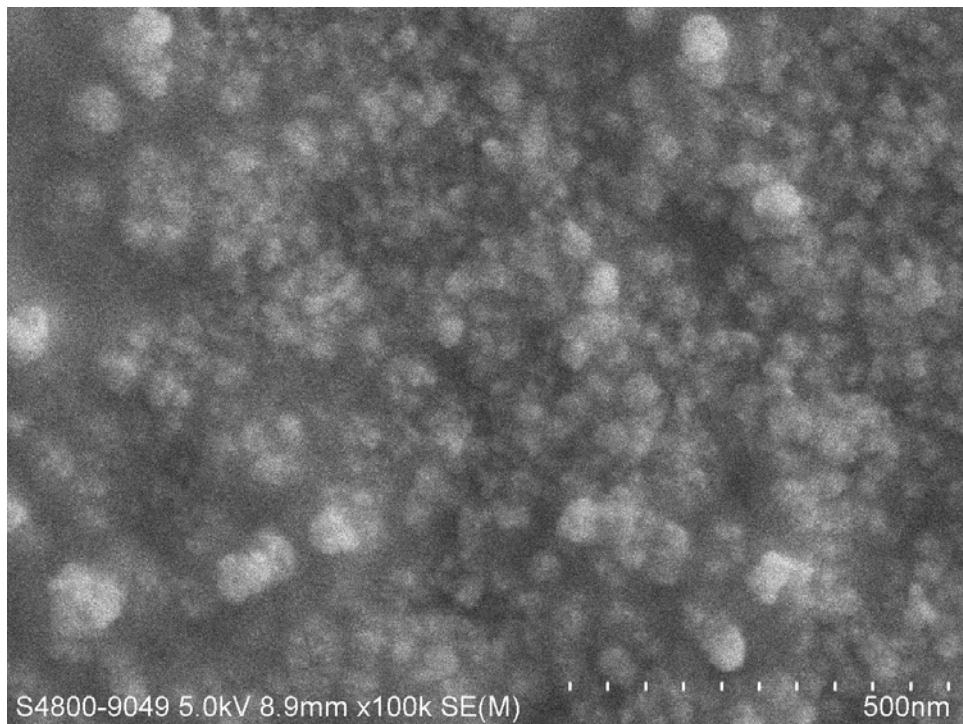
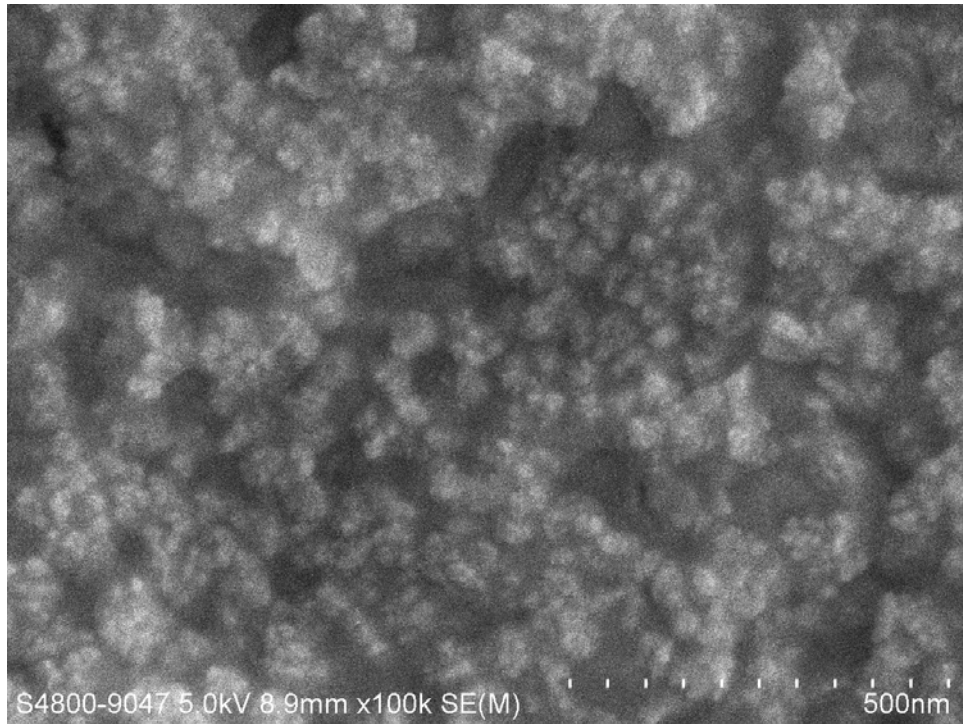


Fig. S2. SEM images of the CdS/ZnS thin film coated on the glass slide before (top) and after (bottom) the photocatalytic hydrogen production test.

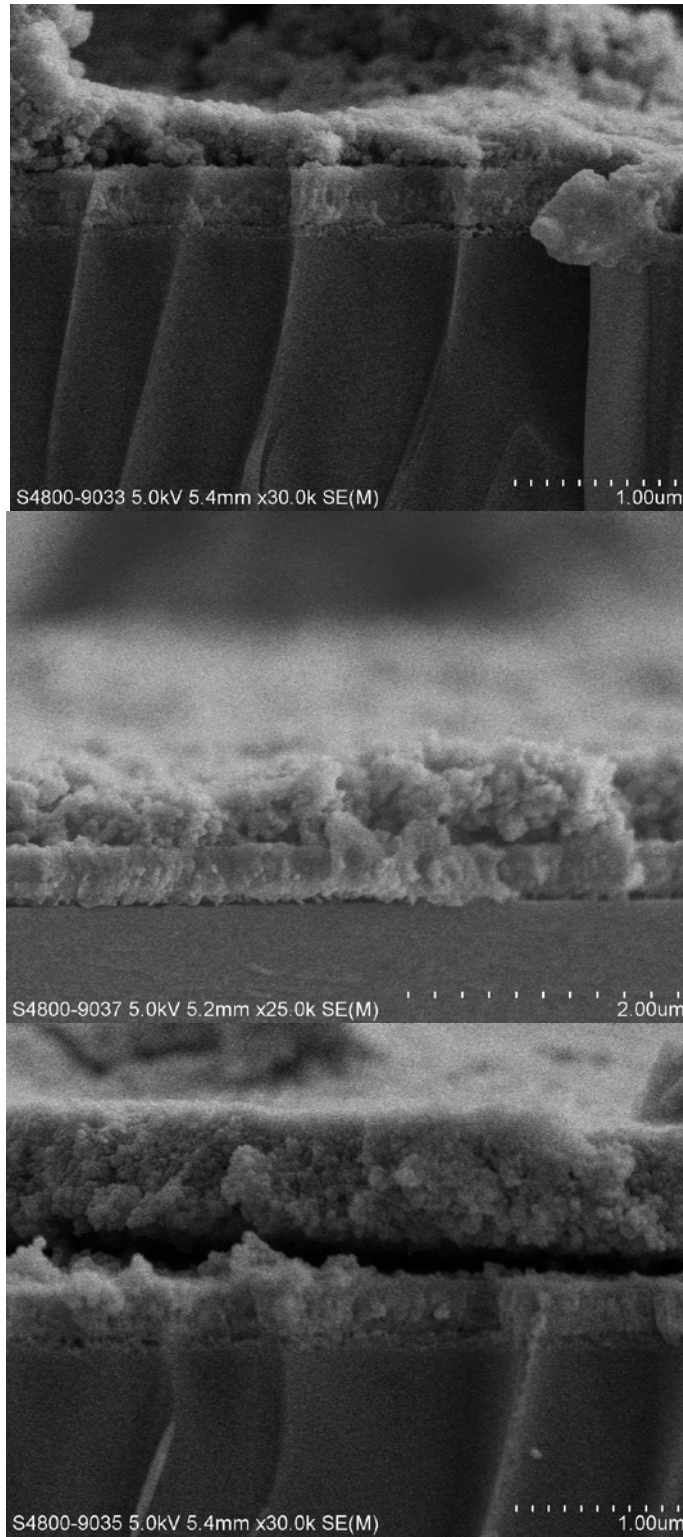


Fig. S3. SEM images of the ZnS layer deposited on the surface of the CdS layer on the glass at different deposition temperatures (top: 40 °C, middle: 50 °C, and bottom: 60 °C).

Table S1. The thickness and roughness of the double-layer CdS/ZnS thin film on glass detected by the AFM before and after the photocatalytic hydrogen production tests.

	Thickness (nm)	Roughness (nm)
Before photo-test	150±7	12.9±2.1
After photo-test	148±8	13.3±1.6